Differential Equations and Dynamical Systems

(International Journal for Theory, Real World Modelling and Simulations)

ISSN: 0971-3514 (print version)

ISSN: 0974-6870 (electronic version)

Publisher: Springer

Accepted January 10th 2019

Lie Group Analysis of Nanofluid Slip Flow with Stefan Blowing Effect via Modified Buongiorno's Model: Entropy Generation Analysis

Puneet Rana[1], Nisha Shukla[1], O. Anwar Bég[2] and Anuj Bhardwaj[1*]

[1]*Department of Mathematics, Jaypee Institute of Information Technology, A-10, Sector-62, Noida-201307, Uttar Pradesh,* ***India.***

[2]*Fluid Mechanics& Propulsion, Aeronautical and Mechanical Engineering, School of Computing, Science & Engineering, University of Salford, Newton Building, M54WT,* ***UK.***

Abstract: This article presents a detailed theoretical and computational analysis of alumina and titania-water nanofluid flow from a horizontal stretching sheet. At the boundary of the sheet (wall), velocity slip, thermal slip and Stefan blowing effects are considered. The Pak-Cho viscosity and thermal conductivity model is employed together with the non-homogeneous Buongiorno nanofluid model. The equations for mass, momentum, energy and nanoparticle species conservation are transformed via Lie-group transformations into a dimensionless system. The partial differential boundary value problem is therefore rendered into nonlinear ordinary differential form. With appropriate boundary conditions, the emerging normalized equations are solved with the semi-numerical homotopy analysis method (HAM). To consider entropy generation affects a second law thermodynamic analysis is also carried out. The impact of some physical parameters on the skin friction, Nusselt number, velocity, temperature and entropy generation number (EGM) are represented graphically. This analysis shows that diffusion parameter is a key factor to retards the friction and rate of heat transfer at the surface. Further, temperature of fluid decreases for the higher value of thermal slip parameter. In addition, entropy

[*]Corresponding author email: anujbhardwaj8@gmail.com, puneetranaiitr@gmail.com (First author)
Contact No.: +91-9711333514

generation number enhances with nanoparticles ambient concentration and Reynolds number. A numerical validation of HAM results is also included. The computations are relevant to thermodynamic optimization of nano-material processing operations.

Keywords: *Nanofluid; HAM; Entropy generation analysis; Stefan blowing effect; Slip flow.*

Nomenclature

C	Nanoparticles Concentration (--)	Pr	Prandtl number (--)
D_B	Brownian Diffusion (m^2 /s)	q	Embedding Parameter (--)
D_T	Thermophoresis Diffusion (m^2 /s)	R	Gas Constant (J/(molK))
D	Ratio of Thermophoresis and Brownian Motion Parameter	Re	Reynolds Number (--)
Ec	Eckert Number (--)	ϕ	Dimensionless Concentration(--)
F	Dimensionless Stream function (--)	S_g	Volumetric rate of entropy generation (J/(Km^3s))
H	Enthalpy (J)	S_c	Characteristic entropy (J/(Km^3s))
K	Thermal Conductivity (W/(mK))	Sc	Schmidt Number (--)
Nur	Nusselt Number(--)	T	Temperature (K)
N_1	Velocity Slip Parameter (--)	u	Velocity (m/s) along x-*axis*
N_2	Thermal Slip Parameter (--)	v	Velocity (m/s) along y -*axis*

Greek Symbol

ρ	Density (kg/m^3)	(ρc)	Heat Capacity (J/(Km^3))

μ	Dynamic Viscosity (Ns/m^2)	θ	Dimensionless Temperature (--)
ϕ	Concentration(--)	χ	Diffusive Constant (--)
ψ	Stream Function (m^2/s)	λ_1	Dimensionless Velocity slip parameter
υ	Kinematic Viscosity (m^2/s)	λ_2	Dimensionless Thermal slip parameter
δ	Thermal Slip Parameter (--)	η	Similarity Variable (--)
	Subscript		
∞	Ambient condition	nf	Nanofluid
w	Condition on surface	f	Fluid
P	Nanoparticles		

1. INTRODUCTION

Heat and mass transfer from a stretching sheet features in a wide area of applications including crystal growth process, paper drying, aerodynamic extrusion of plastic sheets, glass fiber stretching, enrobing, packaging, hot rolling processes, thermal coating flows. Crane[1] initiated theoretical investigations of the boundary layer flow induced by a linearly stretching sheet for the case of a Newtonian viscous fluid. Subsequent investigations have extended this original formulation to consider a multiplicity of effects motivated by achieving a more realistic representation of industrial stretching (polymeric) flows. These include stretching sheet flows for viscoelastic fluids with slip and heat transfer effects [2], new families of Newtonian solutions with wall transpiration [3], multi-mode heat transfer with electrically-conducting and buoyancy effects

[4], uniform-shear free stream effects [5], magnetic rheological behavior [6] , combined free and forced convection for exponential stretching rates [7].

In recent years nanofluids have emerged as a significant area of development in thermal engineering systems. Comprising either metallic or non-metallic nanoscale particles suspended in a conventional working fluid (air, water etc.), nanofluids achieve significant enhancement in thermal conductivities and other properties. Choi and Eastman [2] pioneered this field, describing successful methods for doping base fluids with nano-sized particles which increase the cooling efficiency and thermal conductivity of fluid. The particles of carbon, metal, metal oxides are generally used as nanoparticles. Extensive experimental and theoretical studies have been conducted to evaluate the effect of nanoparticles volume fraction on thermal conductivity of different nanofluids for different applications. Eastman *et al*.[3] observed a 60% enhancement in thermal conductivity by utilizing5% volume fraction of *Cu*, Al_2O_3 and *CuO* nanoparticles. Aybar *et al*. [4] have highlighted that temperature, volume fraction of nanoparticles, size of particles and nano-layer are the important parameters contributing to the increase in thermal conductivity of nanofluids. Rana *et al.* [5] have captured the dual solutions in Jeffery-Hamel nanofluid flow using KKL model. A number of articles are published based on the convective transport study of nanofluid due to its vast industrial applications [6]–[9].

Mathematical models for nanofluid transport can be delineated into two types*: homogeneous* and *non-homogeneous* flow model. In the homogeneous model, the thermo-physical properties of base fluid are increased due to the supplementary nanoparticle thermal conductivity. In the non-homogeneous model proposed by Buongiorno[10] in 2006, although seven mechanisms are identified that may possibly contribute to the heat transfer enhancement, only thermophoresis and

Brownian motion are considered to be substantial. In the past decade a tremendous degree of research activity has been mobilized in nanofluid simulations using these two approaches, for numerous geometries and with multiple body forces, and the reader is referred to [11]–[16]. Yang *et al*.[17] have modified the Buongiorno model to investigate the impact of nanoparticle volume fraction distribution on the conservation equations of mass, momentum and energy which are formulated for the specific case of forced convection flow of nanofluid in a concentric annuals. Malvandi *et al*. [18] have also employed a modified Buongiorno model to investigate the mixed convection nanofluid flow through an annular pipe with buoyancy and hydrodynamic slip effects. Recently, Rana *et al*.[19] have applied the modified Buongiorno model to study the influence of magnetic field, nanoparticles concentration, velocity and thermal slip on electrically-conducting nanofluid flow in external boundary layer flow from a horizontal shrinking cylinder, identifying two branches of solutions. Slip effects are known to arise in various polymeric and other chemical engineering flow systems. An important study of slip conditions at the wall was presented by Yoshimura and Prudhomme [20] in 1988. They observed that the fluid has a velocity relative to the boundary which is known as *slip velocity*.

In many process, it has been observed that there exist mass transfer of species at the surface which can generate a blowing effect. The concept of the blowing effect originates in the Stefan problem[21]. This blowing effect can arise at an impermeable surface and is therefore fundamentally different to the wall transpiration effect associated with injection at permeable surfaces. The Stefan blowing effect provides a relation between the velocity field and the species (concentration) field which states that flow field is directly proportional to the rate of concentration of species. Fang and Jing[22] have considered the Stefan blowing effect on a viscous fluid flow induced by a stretching sheet and observed an improvement in velocity and concentration profiles

due to this effect. Uddin *et al.*[23] analyzed the blowing effect on bioconvection nanofluid flow over a sheet with slip conditions at the wall. They observed a significant modification in velocity, temperature and nanoparticles concentration with blowing parameter. Further, Latiff *et al*. [24] have extended this work to unsteady forced convection nanofluid flow containing microorganism over a rotating stretchable disk. Recently, Rana *et al.*[25] have examined the blowing effect on an electromagnetic time dependent flow of nanofluid induced by a stretching sheet with first order chemical reaction effect.

A flow system can lose its working efficiency due to the presence of thermodynamic irreversibility which can be generated via heat transfer, viscous dissipation and diffusion of species. Entropy generation analysis is a modern tool based on the second law of thermodynamics which provides information about the quantification of this irreversibility. Bejan [26] originated the method of entropy minimization in thermal systems. A diverse spectrum of studies have subsequently been communicated on entropy generation analysis of boundary layer flows external to various different geometries including stretching sheets, cylinders, wedges, spheres etc.[27]–[31]. Moreover, Bhatti *et al.*[30], [32] have examined the study of entropy generation on nanofluid flow induced via a permeable stretching surface.

The major objective of the current article is to determine semi-numerical solutions for Al_2O_3-water nanofluid slip flow from a stretching sheet with Stefan blowing effect using a modified Buongiorno model. The homotopy analysis method [32]–[34] which demonstrates exceptional accuracy for nonlinear coupled ordinary and partial differential equation boundary value problem systems is applied to solve the dimensionless system of flow, energy and concentration equations. Comprehensive evaluation is included for the influence of dominant physical parameters on

velocity, temperature, concentration, skin friction coefficient, Nusselt number and entropy generation number. The study is relevant to thermodynamic optimization of nanomaterial fabrication systems.

2. MATHEMATICAL MODEL

Incompressible steady-state boundary layer flow of Al_2O_3 - water nanofluid is considered along a stretching sheet under the influence of Stefan blowing, velocity slip and thermal slip at the boundary. The $x-axis$ is located along the sheet whereas the $y-axis$ is considered normal to the sheet. It is assumed that sheet is stretched with velocity $u_w = ax$. The physical configuration is illustrated in **Fig 1**.

The concentration of nanoparticles is controlled by no flux condition at the boundary. **Table-1** represents the thermo-physical properties of Al_2O_3 particles and water. A schematic diagram of problem is shown in **Fig.**1. Under these assumptions, four conservation equations can be written following [18] as:

Mass Conservation Equation

$$\frac{\partial}{\partial x}\left(\rho_{nf}u\right)+\frac{\partial}{\partial y}\left(\rho_{nf}v\right)=0, \tag{1}$$

Momentum Conservation Equation

$$u\frac{\partial u}{\partial x}+v\frac{\partial u}{\partial y}=\frac{1}{\rho_{nf}}\frac{\partial}{\partial y}\left(\mu_{nf}\left(\phi\right)\frac{\partial u}{\partial y}\right), \tag{2}$$

Energy Conservation Equation

$$\rho_{nf}\left(u\frac{\partial T}{\partial x}+v\frac{\partial T}{\partial y}\right)=\frac{\partial}{\partial y}\left(k_{nf}\left(\phi\right)\frac{\partial T}{\partial y}\right)+\left(\rho c\right)_p\left(D_B\frac{\partial T}{\partial y}\frac{\partial C}{\partial y}+D_T\frac{1}{T_\infty}\left(\frac{\partial T}{\partial y}\right)^2\right) \tag{3}$$

Nanoparticles Mass Conservation Equation

$$u\frac{\partial C}{\partial x}+v\frac{\partial C}{\partial y}=\frac{\partial}{\partial y}\left[D_B\frac{\partial C}{\partial y}+\frac{D_T}{T_\infty}\frac{\partial T}{\partial y}\right]. \tag{4}$$

Boundary Conditions[36]

At $y=0,\ u=u_w+N_1\frac{\partial u}{\partial y},\ v=-D_B\frac{\partial C}{\partial y},\ T=T_w+N_2\frac{\partial T}{\partial y},\ D_B\frac{\partial C}{\partial y}+\frac{D_T}{T}\frac{\partial T}{\partial y}=0,$

as $y\to\infty,\ u=0,\ T=T_\infty,\ C=C_\infty.$ (5)

where u (m/s)and v(m/s) are the velocities along the x and *y-axis* respectively, ρ_{nf} (kg/m^3) is density of nanofluid, μ_{nf} (N-s/m^2) is dynamic viscosity of nanofluid, H(J) is enthalpy, k_{nf} (W/m-K) is thermal conductivity of nanofluid, T and T_∞ (K) are temperature of nanofluid and ambient temperature respectively, $\left(\rho c\right)_p$ (J/K-m^3)is heat capacity of nanoparticles, D_B and D_T (m^2/s) are Brownian and thermophoresis diffusion respectively, C and C_∞ are the nanoparticles concentration and ambient concentration respectively, N_1 and N_2 (m) are the velocity and thermal slip parameter, T_w (K) is the temperature at the wall which is assumed to be greater in comparison of ambient temperature $\left(T_w>T_\infty\right)$.

2.1 The Thermo-physical Properties

The density and heat capacity of nanofluid are defined as:

$$\rho_{nf} = \phi\rho_p + (1-\phi)\rho_f, \tag{6}$$

$$(\rho c)_{nf} = \phi(\rho c)_p + (1-\phi)(\rho c)_f. \tag{7}$$

Here the suffix *nf* stands for nanofluid whereas *f* represents the base fluid. The symbol ϕ represents the concentration of nanoparticles. Pak and Cho[37] have measured the viscosity and thermal conductivity of nanofluid at room temperature deriving the following relations:

2.1.1. Alumina Particles

$$\mu_{nf} = \mu_f(1+39.11\phi+533.9\phi^2), \tag{8}$$

$$k_{nf} = k_f(1+7.47\phi). \tag{9}$$

2.1.2 Titania Nanoparticles

$$\mu_{nf} = \mu_f(1+5.45\phi+108.2\phi^2), \tag{10}$$

$$k_{nf} = k_f(1+2.92\phi-11.99\phi^2). \tag{11}$$

2.2 Normalization of governing equations

To normalize the transport equations, we introduce following dimensionless variables:

$$x^* = x\sqrt{\frac{a}{\upsilon_f}},\ y^* = y\sqrt{\frac{a}{\upsilon_f}},\ u^* = \frac{u}{\sqrt{a\upsilon_f}},\ v^* = \frac{v}{\sqrt{a\upsilon_f}},\ \theta = \frac{T-T_\infty}{T_w-T_\infty},\ \phi = C. \tag{12}$$

The stream function can be defined as $u^* = \frac{\partial \psi}{\partial y^*}$, $v^* = -\frac{\partial \psi}{\partial x^*}$. Applying eqn. (12) on eqs.(1)-(5), yields:

$$\frac{\mu_{nf}}{\mu_f}\frac{\partial^3 \psi}{\partial y^{*3}} + \frac{1}{\mu_f}\frac{\partial \mu_{nf}}{\partial \phi}\frac{\partial \phi}{\partial y^*}\frac{\partial^2 \psi}{\partial y^{*2}} + \frac{\rho_{nf}}{\rho_f}\left(\frac{\partial \psi}{\partial x^*}\frac{\partial^2 \psi}{\partial y^{*2}} - \frac{\partial \psi}{\partial y^*}\frac{\partial^2 \psi}{\partial x^* \partial y^*}\right) = 0, \tag{13}$$

$$\frac{k_{nf}}{k_f}\frac{\partial^2 \theta}{\partial y^{*2}} + \frac{1}{k_f}\frac{\partial k_{nf}}{\partial \phi}\frac{\partial \theta}{\partial y^*}\frac{\partial \phi}{\partial y^*} + \frac{(\rho c)_p}{(\rho c)_f}\frac{\mathrm{Pr}}{Sc}\left(\frac{\partial \theta}{\partial y^*}\frac{\partial \phi}{\partial y^*} + D\left(\frac{\partial \theta}{\partial y^*}\right)^2\right) + \mathrm{Pr}\frac{(\rho c)_{nf}}{(\rho c)_f}\left(\frac{\partial \psi}{\partial x^*}\frac{\partial \theta}{\partial y^*} - \frac{\partial \psi}{\partial y^*}\frac{\partial \theta}{\partial x^*}\right) = 0, \tag{14}$$

$$\frac{\partial^2 \phi}{\partial y^{*2}} + Sc\left(\frac{\partial \psi}{\partial x^*}\frac{\partial \phi}{\partial y^*} - \frac{\partial \phi}{\partial x^*}\right) + D\frac{\partial^2 \theta}{\partial y^{*2}} = 0, \tag{15}$$

The following boundary conditions enforced at the wall and in the free stream are:

$$\text{At } y^* = 0,\ \frac{\partial \psi}{\partial y^*} = ax^* + N_1\sqrt{\frac{a}{\upsilon_f}}\frac{\partial^2 \psi}{\partial y^{*2}},\ \frac{\partial \psi}{\partial x^*} = \frac{1}{Sc}\frac{\partial \phi}{\partial y^*},\ \theta = 1 + N_2\sqrt{\frac{a}{\upsilon_f}}\frac{\partial \theta}{\partial y^*},\ \frac{\partial \phi}{\partial y^*} + D\frac{\partial \theta}{\partial y^*} = 0,$$

$$\text{As } y^* \to \infty\ \frac{\partial \psi}{\partial y^*} = 0,\ \theta = 0,\ \phi = C_\infty. \tag{16}$$

2.3 Lie group analysis of normalized equations

To convert the partial differential equations (13)-(16) into ordinary differential equations, we deploy the following scaling group of transformations:

$$x^* = e^{-\varepsilon k_1}\bar{x},\ y^* = e^{-\varepsilon k_2}\bar{y},\ \psi^* = e^{-\varepsilon k_3}\bar{\psi},\ \theta^* = e^{-\varepsilon k_4}\bar{\theta},\ \phi^* = e^{-\varepsilon k_5}\bar{\phi},\ N_1 = e^{-\varepsilon k_6}\bar{N}_1 \text{ and } N_2{}^* = e^{-\varepsilon k_7}\bar{N}_2. \tag{17}$$

Here all k_i's are constants and the symbol *s* used to indicate the scaling group parameter. Apply the transformations (17) on eqns. (13)-(16) then we obtain:

$$\frac{\mu_{nf}}{\mu_f}\frac{\partial^3\bar{\psi}}{\partial\bar{y}^3}e^{-\varepsilon(k_3-3k_2)}+\frac{1}{\mu_f}\frac{\partial\mu_{nf}}{\partial\bar{\phi}}\frac{\partial\bar{\phi}}{\partial\bar{y}}\frac{\partial^2\bar{\psi}}{\partial\bar{y}^2}e^{-\varepsilon(k_3-3k_2+k_5)}+\frac{\rho_{nf}}{\rho_f}\left(\frac{\partial\bar{\psi}}{\partial\bar{x}}\frac{\partial^2\bar{\psi}}{\partial\bar{y}^2}-\frac{\partial\bar{\psi}}{\partial\bar{y}}\frac{\partial^2\bar{\psi}}{\partial\bar{x}\partial\bar{y}}\right)e^{-\varepsilon(2k_3-k_1-2k_2)}=0, \tag{18}$$

$$\frac{k_{nf}}{k_f}\frac{\partial^2\bar{\theta}}{\partial\bar{y}}e^{-\varepsilon(k_4-2k_2)}+\frac{1}{k_f}\frac{\partial k_{nf}}{\partial\bar{\phi}}\frac{\partial\bar{\theta}}{\partial\bar{y}}\frac{\partial\bar{\phi}}{\partial\bar{y}}e^{-\varepsilon(k_4-2k_2+k_5)}+\frac{(\rho c)_p}{(\rho c)_f}\frac{\Pr}{Sc}\left(\frac{\partial\bar{\theta}}{\partial\bar{y}}\frac{\partial\bar{\phi}}{\partial\bar{y}}e^{-\varepsilon(k_4+k_5-2k_2)}+D\left(\frac{\partial\bar{\theta}}{\partial\bar{y}}\right)^2e^{-\varepsilon 2(k_4-k_2)}\right)$$

$$+\Pr\frac{(\rho c)_{nf}}{(\rho c)_f}\left(\frac{\partial\bar{\psi}}{\partial\bar{x}}\frac{\partial\bar{\theta}}{\partial\bar{y}}-\frac{\partial\bar{\psi}}{\partial\bar{y}}\frac{\partial\bar{\theta}}{\partial\bar{x}}\right)e^{-\varepsilon(k_3+k_4-k_1-k_2)}=0, \tag{19}$$

$$\frac{\partial^2\bar{\phi}}{\partial\bar{y}^2}e^{-\varepsilon(k_5-2k_2)}+Sc\left(\frac{\partial\bar{\psi}}{\partial\bar{x}}\frac{\partial\bar{\phi}}{\partial\bar{y}}e^{-\varepsilon(k_3+k_5-k_1-k_2)}-\frac{\partial\bar{\phi}}{\partial\bar{x}}e^{-\varepsilon(k_5-k_1)}\right)+D\frac{\partial^2\bar{\theta}}{\partial\bar{y}^2}e^{-\varepsilon(k_4-2k_2)}=0, \tag{20}$$

The corresponding boundary conditions are:

$$\text{at } \bar{y}=0,\ \frac{\partial\bar{\psi}}{\partial\bar{y}}e^{-\varepsilon(k_3-k_2)}=a\bar{x}e^{-\varepsilon k_1}+\bar{N}_1e^{-\varepsilon k_6}\sqrt{\frac{a}{\upsilon_f}}\frac{\partial^2\bar{\psi}}{\partial\bar{y}^2}e^{-\varepsilon(k_3-2k_2)},\ \ \frac{\partial\bar{\psi}}{\partial\bar{x}}e^{-\varepsilon(k_3-k_1)}=\frac{1}{Sc}\frac{\partial\bar{\phi}}{\partial\bar{y}}e^{-\varepsilon(k_5-k_2)},$$

$$\bar{\theta}e^{-\varepsilon k_4}=1+\bar{N}_2e^{-\varepsilon k_7}\sqrt{\frac{a}{\upsilon_f}}\frac{\partial\bar{\theta}}{\partial\bar{y}}e^{-\varepsilon(k_4-k_2)},\ \frac{\partial\bar{\phi}}{\partial\bar{y}}e^{-\varepsilon(k_5-k_2)}+D\frac{\partial\bar{\theta}}{\partial\bar{y}}e^{-\varepsilon(k_4-k_2)}=0$$

$$\text{as } \bar{y}\to\infty\ \frac{\partial\bar{\psi}}{\partial\bar{y}}e^{-\varepsilon(k_3-k_2)}=0,\ \bar{\theta}e^{-\varepsilon k_4}=0,\ \bar{\phi}e^{-\varepsilon k_5}=C_\infty. \tag{21}$$

To maintain non-variance of the above system of differential equations under the group of transformations, we obtain following relations:

$$2k_3 - k_1 - 2k_2 = k_3 - 3k_2 = k_3 - 3k_2 + k_5 = k_3 - 3k_2 + 2k_5 \tag{22}$$

$$k_3 + k_4 - k_1 - k_2 = k_4 - 2k_2 = k_4 - 2k_2 + k_5 = 2(k_4 - k_2) \tag{23}$$

$$k_5 - k_1 = k_3 + k_5 - k_1 - k_2 = k_5 - 2k_2 = k_4 - 2k_2 \tag{24}$$

$$k_3 - k_2 = k_1 = k_3 - 2k_2 + k_6 \tag{25}$$

$$k_3 - k_1 = k_5 - k_2 \tag{26}$$

$$k_4 = 0 = k_4 - k_2 + k_7 \tag{27}$$

$$k_5 - k_2 = k_4 - k_2 \tag{28}$$

The above eqns. (22)-(28) provide the solutions:

$$k_1 = k_3,\ k_2 = 0,\ k_4 = 0,\ k_5 = k_4,\ k_6 = 0,\ k_7 = k_2. \tag{29}$$

Substitute the values of all k_i'*s* into the transformations (17) leads to:

$$x^* = e^{-\varepsilon k_1}\bar{x},\ \ y^* = \bar{y}, \psi^* = e^{-\varepsilon k_1}\bar{\psi},\ \theta^* = \bar{\theta},\ \phi^* = \bar{\phi},\ N_1 = \bar{N}_1 \text{ and } N_2{}^* = \bar{N}_2. \tag{30}$$

Next, we employ Taylor series to expand the above terms up to order ε, leading to:

$$\frac{dx}{x} = \frac{dy}{0} = \frac{d\psi}{\psi} = \frac{d\theta}{0} = \frac{d\phi}{0} \tag{31}$$

which provides the following transformations

$$\eta = y,\ \psi = xf(\eta),\ \theta = \theta(\eta) \text{ and } \phi = \phi(\eta). \tag{32}$$

Now apply non-dimensional parameters (32) on eqs. (1)-(5), then we obtain:

$$\frac{\mu_{nf}}{\mu_f} f''' + \frac{1}{\mu_f}\frac{\partial \mu_{nf}}{\partial \phi}\phi' f'' + \frac{\rho_{nf}}{\rho_f}\left(ff'' - f'^2 \right) = 0, \tag{33}$$

$$\frac{k_{nf}}{k_f}\theta'' + \frac{1}{k_f}\frac{\partial k_{nf}}{\partial \phi}\theta'\phi' + \frac{(\rho c)_p}{(\rho c)_f}\frac{\Pr}{Sc}\left(\theta'\phi' + D\theta'^2\right) + \Pr\frac{(\rho c)_{nf}}{(\rho c)_f} f\theta' = 0, \tag{34}$$

$$\phi'' + Scf\phi' + D\theta'' = 0, \tag{35}$$

The boundary conditions emerge as:

$$\text{at } \eta = 0,\ f(0) = \frac{1}{Sc}\phi'(0),\ f'(0) = 1 + \lambda f''(0),\ \theta(0) = 1 + \delta\theta'(0),\ \phi'(0) + D\theta'(0) = 0,$$

$$\text{as } \eta \to \infty,\ f'(\eta) = 0,\ \theta(\eta) = 0,\ \phi(\eta) = C_\infty, \tag{36}$$

Here prime/ designates differentiation with respect to η and the leading parameters can be defined as:

$$\Pr = \frac{\mu_f c_f}{k_f},\ Sc = \frac{\upsilon_f}{D_B},\ D = \frac{D_T\left(T_w - T_\infty\right)}{T_\infty D_B},\ \lambda = N_1\sqrt{\frac{a}{\upsilon_f}},\ \delta = N_2\sqrt{\frac{a}{\upsilon_f}}. \tag{37}$$

Where *Pr* is Prandtl number, *Sc* is Schmidt number, *D* is diffusivity ratio, γ is first order hydrodynamic slip parameter and δ is thermal slip (jump) parameter.

2.4 The Significant Engineering Quantities of Interest

Of relevance to materials processing operation design are the gradients of variables at the wall (sheet surface). These are defined for the momentum, temperature and nanoparticle concentration fields below:

2.4.1 Skin Friction Coefficient

$C_f = \dfrac{\tau_w}{\rho_f u_w^2}$, where the shear stress τ_w is defined as $\tau_w = \mu_{nf} \left.\dfrac{\partial u}{\partial y}\right|_{y=0}$.

Now, apply the transformations (32) on the expression of C_f, then we obtain

$$C_{fr} = \sqrt{\mathrm{Re}} C_f = \frac{\mu_{nf}}{\mu_f} f''(0), \tag{38}$$

where the local Reynolds number $\mathrm{Re} = \dfrac{ax^2}{\upsilon_f}$.

2.4.2 Local Nusselt Number

$Nu = \dfrac{x}{k_f (T_w - T_\infty)} q_w$, where the heat flux at the wall q_w is defined as

$q_w = -k_{nf} \dfrac{\partial T}{\partial y} + H j_p$, where the mass flux j_p is defined as

$$j_p = -\rho_p \left(D_B \frac{\partial C}{\partial y} + \frac{D_T}{T} \frac{\partial T}{\partial y} \right)_{y=0}.$$

Use eq. (32) on the expression of *Nu*, then we obtain

$$Nur = \frac{Nu}{\sqrt{\mathrm{Re}}} = -\frac{k_{nf}}{k_f} \theta'(0). \tag{39}$$

2.2.3 Sherwood Number

$Sh = \frac{xq_m}{D_B}$, where the mass flux q_m is defined as

$$q_m = \frac{j_p}{\rho_p}.$$

Since j_p is zero at the boundary thus Sherwood number is zero.

3. Second Law Thermodynamic Analysis (Entropy Generation Minimization)

The second law of thermodynamics provides a mechanism for computing the entropy generation in the system. For the present problem, the *volumetric rate of entropy generation* is defined as [31]:

$$S_g = \frac{k_{nf}}{T_\infty^2}\left(\frac{\partial T}{\partial y}\right)^2 + \frac{\mu_{nf}}{T_\infty}\left(\frac{\partial u}{\partial y}\right)^2 + RD_B\left(\frac{\partial C}{\partial y}\right)^2 + \frac{RD_B}{T_\infty}\left(\frac{\partial C}{\partial y}\right)\left(\frac{\partial T}{\partial y}\right), \tag{40}$$

$$= S_1 + S_2 + S_3 + S_4,$$

where S_1 is the entropy generation due to *temperature difference*, S_2 is the entropy generation due to *viscous dissipation* and the combination of the last two terms $S_3 \& S_4$ represents the entropy generation due to *diffusion of species*. Here *R* represents the gas constant (J $mol^{-1}K^{-1}$).

The characteristic entropy generation is given by:

$$S_c = \frac{k_f \left(T_w - T_\infty\right)^2}{x^2 T_\infty^2}. \tag{41}$$

Using similarity transformations (32) on the ratio of S_g and S_c, yields a *non-dimensional entropy generation number*:

$$Ns = \frac{S_g}{S_c} = \mathrm{Re}\left(\frac{k_{nf}}{k_f}\theta'^2 + \frac{\mu_{nf}}{\mu_f}\mathrm{Pr}\, Ecf''^2 + \frac{\chi}{\Omega}\left(\frac{1}{\Omega}\phi'^2 + \theta'\phi' \right) \right) = Ns_t + Ns_v + Ns_d, \tag{42}$$

where $\chi = \frac{RD_B}{k_f}$, $Ec = \frac{u_w^2}{c_f(T_w - T_\infty)}$ and $\Omega = \frac{T_w - T_\infty}{T_\infty}$. These denote respectively the thermodynamic parameter, Eckert (viscous heating) parameter and wall-free stream temperature difference parameter. The relative entropy generation number of temperature (Bejan number, Ns_{rt}) can be calculated as the ratio of Ns_t and total entropy. Similarly, other relative entropy generation numbers Ns_{rv} and Ns_{rd} may be defined. Bejan number [26], [28] represents the *relative entropy generation number of temperature difference* which is the ratio of Ns_t to *Ns*. In a similar fashion it is possible to determine the other relative entropy generation numbers.

4. Semi-Numerical Solution of BVP with Homotopy Analytical Technique

To solve the eqns. (33)-(35)under boundary conditions (36), we employ Liao's homotopy analysis method (HAM)for which the initial guesses, linear operators and auxiliary functions are assumed as follows [38]:

(i)Initial guesses $f_0(\eta) = \frac{D}{Sc(1+\delta)} + \frac{1}{1+\lambda}\left(1 - e^{-\eta}\right)$, $\theta_0(\eta) = \frac{1}{1+\delta}\mathrm{e}^{-\eta}$, $\phi_0(\eta) = C_\infty - \frac{D}{1+\delta}\mathrm{e}^{-\eta}$,

which satisfy the boundary conditions (36).

(ii)The linear operators $L_f = f''' + f'', L_\theta = \theta'' + \theta', L_\phi = \phi'' + \phi',$ which satisfy the conditions $L_f(C_1 + C_2\eta + C_3 e^{-\eta}) = 0$, $L_\theta(C_4 + C_5 e^{-\eta}) = 0$, $L_\phi(C_6 + C_7 e^{-\eta}) = 0.$ Here C_i are constants.

(iii)The auxiliary functions $H_f(\eta) = 1,\ H_\theta(\eta) = 1,\ H_\phi(\eta) = 1.$

We construct the following m^{th} order deformation equations

$$L_f(f_m(\eta) - \chi_{m-1} f_{m-1}(\eta)) = h_f H_f R_m^f(\eta), \tag{43}$$

$$L_\theta(\theta_m(\eta) - \chi_{m-1}\theta_{m-1}(\eta)) = h_\theta H_\theta R_m^\theta(\eta), \tag{44}$$

$$L_\phi(\phi_m(\eta) - \chi_{m-1}\phi_{m-1}(\eta)) = h_\phi H_\phi R_m^\phi(\eta), \tag{45}$$

at $\eta = 0,\ f_m(0) = \frac{1}{Sc}\phi'(0),\ f_m'(0) - \lambda f_m''(0) = 0,\quad \theta_m(0) - \delta\theta_m'(0) = 0,\ \phi'(0) + D\theta'(0) = 0,$

as $\eta \to \infty,\ f_m'(\eta) = 0,\ \theta_m(\eta) = 0,\ \phi_m(\eta) = 0.$ (46)

In above eqs. h_f , h_θ and h_ϕ are the auxiliary parameters which can be calculated by plotting the *h-curves* with higher order derivatives of $f(\eta), \theta(\eta)$ and $\phi(\eta).$ The functions R_m^f , R_m^θ and R_m^ϕ are defined as

$$R_m^f(\eta) = \frac{1}{m-1!}\frac{\partial^{m-1} N_f(\eta, q)}{\partial q^{m-1}}\bigg|_{q=0}, \ R_m^\theta(\eta) = \frac{1}{m-1!}\frac{\partial^{m-1} N_\theta(\eta, q)}{\partial q^{m-1}}\bigg|_{q=0} \text{ and}$$

$$R_m^\phi(\eta) = \frac{1}{m-1!}\frac{\partial^{m-1} N_\phi(\eta, q)}{\partial q^{m-1}}\bigg|_{q=0}. \tag{47}$$

Here $N_f(\eta,q)$, $N_\theta(\eta,q)$ and $N_\phi(\eta,q)$ are *non-linear operators* which are obtained from eqns. (33)-(35) and q is an embedding parameter which lies between 0 and 1. The value of the function χ_m is 0 for $m \le 1$ otherwise 1.

4.1 Convergence of HAM

Liao [38] emphasized the crucial role played by the auxiliary parameters in ensuring convergence of HAM series solutions. In present problem, we have sketched the *h-curves* with $f''(0)$, $\theta'(0)$ and $\phi'(0)$ for different order of approximations which are shown in **Fig.2**. This figure represents a horizontal line in the ranges $h_f = [-0.014 \quad -0.003]$, $h_\theta = [-0.015 \quad -0.0005]$ and $h_\phi = [-0.018 \quad 0]$. Thus, we have selected $h_f = -0.011$, $h_\theta = -0.0013$, $h_\phi = -0.002$ and checked the order of convergence upto twenty five order of approximations which is shown in **Table-2**. This table ensures that the convergence of solution series is achieved at twenty two order of approximations.

5. RESULTS AND DISCUSSION

To provide an insight into the momentum, thermal, nano-particle species and entropy generation characteristics for the current regime i.e. Al_2O_3-water nanofluid flow induced by stretching sheet, extensive computations have been performed with HAM in the symbolic software MAPLE. The values of the featured parameters are prescribed as follows (unless otherwise indicated): $\lambda = 0.1$, $\delta = 0.1$, $C_\infty = 0.05$, $Sc = 10$, $\mathrm{Re} = 10$, $\mathrm{Pr} = 6.2$, $D = 0.001$, $Ec = 0.01$, $\chi = 30.1142 \times 10^{-9}$ and $\Omega = 0.03$. **Table-3** provides the comparison of HAM results with shooting (numerical quadrature)

and evidently very good correlation is attained. Confidence in the present HAM results is therefore high. The effect of several key parameters on velocity, temperature, concentration, skin friction, Nusselt number and entropy generation number are visualized graphically.

Fig. 3 (a) represents the velocity profile for different values of velocity slip parameter λ which indicates that velocity is depleted slightly with increasing λ. A similar result is obtained from **Fig. 3(b)** which demonstrates a reduction in temperature with increasing thermal slip parameter. Therefore greater wall hydrodynamic slip increases momentum boundary layer thickness whereas increasing thermal slip reduces thermal boundary layer thickness. **Fig. 3(c)** reveals the impact of diffusion parameter *D* on the distribution of nano-particle concentration. Clearly there is a significant decrease in concentrations with a rise in the value of diffusion parameter again manifesting in a decrease in species boundary layer thickness. **Fig.4** shows the influence of different metallic nanoparticles on velocity and temperature distributions. Both velocity and temperature are greater for Al_2O_3-water nanofluid as compared with TiO_2-water nanofluid. Better flow acceleration is therefore achieved with the former as compared to the latter. Furthermore Al_2O_3-water nanofluid achieves greater thermal enhancement or heating efficiency as compare to TiO_2-water nanofluid since thermal conductivity of alumina particles exceeds that of titania particles.

The combined effects of nanoparticle concentration C_∞ and diffusion parameter *D* on skin friction coefficient and Nusselt number are depicted in **Fig.5.** Surface (skin) friction is markedly reduced with an increment in either C_∞ or *D i.e. flow deceleration is induced*. Thus a modification in the value of nanoparticles concentration effectively increases momentum boundary layer thickness

since momentum diffusion is impeded. **Fig. 5(b)** illustrates that Nusselt number is an increasing function of C_∞ whereas it is a decreasing function of *D*. The implication is that a greater nanoparticle concentration enhances heat transfer rate to the wall and therefore depletes thermal energy from the boundary layer resulting in a decrease in thermal boundary layer thickness.

The influence of several physical parameters on entropy generation number is presented in **Fig. 6.** A high value of local Reynolds number can increase the randomness in the system. Thus, entropy increases with an increase in the value of Reynolds number (greater inertial force relative to viscous hydrodynamic force) as depicted in **Fig. 6(a)**. The influence of thermal slip parameter δ on *Ns* is depicted in **Fig. 6 (b)** which indicates that entropy generation number is suppressed with an increase the value of δ . **Fig. 6(c)** shows that *Ns* increases with nanoparticle concentration C_∞ . Hence, a large amount of nanoparticles can enhance the entropy generation in the system. **Fig. 6(d)** illustrates the contribution of different sources of entropy generation (relative entropy generation function). Apparently entropy generation due to thermal diffusion (Bejan number, Ns_{rt}) is a major source in the vicinity of the sheet surface (wall) whereas it is insignificant far away from the surface. The second source of entropy generation, Ns_{rv} is due to viscous dissipation which approaches zero *near the surface of the sheet* whereas it is a dominant source at a large distance from the sheet. Furthermore entropy generation, Ns_{rd} due to the diffusion of nanoparticles exerts a trivial impact at the sheet surface.

Fig.7 depicts the combined influence of physical parameters (C_∞, Ec).and (D, Re) on entropy generation number *Ns*. Entropy generation increases with an increase in nanoparticle concentration C_∞ (in concurrence with **Fig. 6(c)**), Eckert number *Ec* and Reynolds number *Re*(again in agreement with **Fig.6(a)**) whereas it decreases with diffusion parameter *D*.

6. CONCLUSIONS

An analytical study of Al_2O_3-water nanofluid flow induced by a stretching sheethas been presented. The modified two-component Buongiorno model has been deployed. At the surface of the sheet, both velocity slip and thermal slip conditions are imposed. Entropy generation analysis has also been conducted to provide a thermodynamic optimization aspect to the work. The homotopy analysis method has been implemented to solve the dimensionless, transformed system of ordinary differential boundary layer conservation equations which have been derived with the aid of Lie algebraic group methods. The influence of physical parameters velocity (hydrodynamic) slip, thermal slip, nano-particle concentration and species diffusivity (λ , δ , C_∞, D) on velocity, temperature, skin friction coefficient, Nusselt number and entropy generation number has been computed and illustrated graphically. The computations have been validated with a shooting numerical quadrature method available in MATLAB. The important deductions from the present investigation can be summarized as follows:

- Velocity of the nanofluid is observed to be a decreasing function of velocity slip parameter.
- The temperature of nanofluid increases with doping of high thermal conductivity nanoparticles.
- Temperature and entropy generation number are decreased as the value of thermal slip parameter is increased.
- The diffusion parameter reduces the skin friction, Nusselt number and concentration of nanoparticles.
- Entropy generation number and Nusselt number are increased with nanoparticle concentration C_∞ whereas skin friction at the surface of the sheet is decreased.

- Greater local Reynolds number results in an elevation in entropy generation in the system.
- Based on a relative entropy generation analysis, entropy generation is observed to be enhanced with nanoparticle concentration and Eckert number whereas it is depleted with diffusion parameter.

REFERENCES

[1] L. J. Crane, "Flow past a stretching plate," *Z. Für Angew. Math. Phys. ZAMP*, vol. 21, no. 4, pp. 645–647, Jul. 1970.

[2] S. U. S. Choi and J. A. Eastman, "Enhancing thermal conductivity of fluids with nanoparticles," Argonne National Lab., IL (United States), ANL/MSD/CP--84938; CONF-951135--29, Oct. 1995.

[3] J. A. Eastman, U. S. Choi, S. Li, L. J. Thompson, and S. Lee, "Enhanced Thermal Conductivity through the Development of Nanofluids," *Fall Meet. Mater. Res. Soc. MRS Boston USA*, vol. 457, Jan. 1996.

[4] H. Ş. Aybar, M. Sharifpur, M. R. Azizian, M. Mehrabi, and J. P. Meyer, "A Review of Thermal Conductivity Models for Nanofluids," *Heat Transf. Eng.*, vol. 36, no. 13, pp. 1085–1110, Sep. 2015.

[5] P. Rana, N. Shukla, Y. Gupta, and I. Pop, "Analytical prediction of multiple solutions for MHD Jeffery–Hamel flow and heat transfer utilizing KKL nanofluid model," *Phys. Lett. A*, Oct. 2018.

[6] M. Sheikholeslami and H. B. Rokni, "CVFEM for effect of Lorentz forces on nanofluid flow in a porous complex shaped enclosure by means of non-equilibrium model," *J. Mol. Liq.*, vol. 254, pp. 446–462, Mar. 2018.

[7] M. Sheikholeslami, M. Darzi, and M. K. Sadoughi, "Heat transfer improvement and pressure drop during condensation of refrigerant-based nanofluid; an experimental procedure," *Int. J. Heat Mass Transf.*, vol. 122, pp. 643–650, Jul. 2018.

[8] M. Sheikholeslami, "Numerical investigation for CuO-H2O nanofluid flow in a porous channel with magnetic field using mesoscopic method," *J. Mol. Liq.*, vol. 249, pp. 739–746, Jan. 2018.

[9] M. Sheikholeslami and H. B. Rokni, "Numerical simulation for impact of Coulomb force on nanofluid heat transfer in a porous enclosure in presence of thermal radiation," *Int. J. Heat Mass Transf.*, vol. 118, pp. 823–831, Mar. 2018.

[10] J. Buongiorno, "Convective Transport in Nanofluids," *ASME J. Heat Transf.*, vol. 128, no. 3, pp. 240–250, 2006.

[11] R. Dhanai, P. Rana, and L. Kumar, "Critical values in slip flow and heat transfer analysis of non-Newtonian nanofluid utilizing heat source/sink and variable magnetic field: Multiple solutions," *J. Taiwan Inst. Chem. Eng.*, vol. 58, pp. 155–164, Jan. 2016.

[12] R. Dhanai, P. Rana, and L. Kumar, "MHD mixed convection nanofluid flow and heat transfer over an inclined cylinder due to velocity and thermal slip effects: Buongiorno's model," *Powder Technol.*, vol. 288, pp. 140–150, Jan. 2016.

[13] A. V. Kuznetsov and D. A. Nield, “Natural convective boundary-layer flow of a nanofluid past a vertical plate: A revised model,” *Int. J. Therm. Sci.*, vol. 77, pp. 126–129, Mar. 2014.
[14] P. Rana, R. Bhargava, and O. A. Bég, “Numerical solution for mixed convection boundary layer flow of a nanofluid along an inclined plate embedded in a porous medium,” *Comput. Math. Appl.*, vol. 64, no. 9, pp. 2816–2832, Nov. 2012.
[15] P. Rana, R. Bhargava, and O. A. Bég, “Finite element modeling of conjugate mixed convection flow of Al 2 O 3 –water nanofluid from an inclined slender hollow cylinder,” *Phys. Scr.*, vol. 87, no. 5, pp. 1–15, 2013.
[16] M. M. Rashidi, N. Freidoonimehr, A. Hosseini, O. A. Bég, and T.-K. Hung, “Homotopy simulation of nanofluid dynamics from a non-linearly stretching isothermal permeable sheet with transpiration,” *Meccanica*, vol. 49, no. 2, pp. 469–482, Feb. 2014.
[17] C. Yang, W. Li, and A. Nakayama, “Convective heat transfer of nanofluids in a concentric annulus,” *Int. J. Therm. Sci.*, vol. 71, pp. 249–257, Sep. 2013.
[18] A. Malvandi, S. A. Moshizi, E. G. Soltani, and D. D. Ganji, “Modified Buongiorno’s model for fully developed mixed convection flow of nanofluids in a vertical annular pipe,” *Comput. Fluids*, vol. 89, pp. 124–132, Jan. 2014.
[19] P. Rana, R. Dhanai, and L. Kumar, “MHD slip flow and heat transfer of Al2O3-water nanofluid over a horizontal shrinking cylinder using Buongiorno’s model: Effect of nanolayer and nanoparticle diameter,” *Adv. Powder Technol.*, vol. 28, no. 7, pp. 1727–1738, Jul. 2017.
[20] A. Yoshimura and R. K. Prud’homme, “Wall Slip Corrections for Couette and Parallel Disk Viscometers,” *J. Rheol.*, vol. 32, no. 1, pp. 53–67, Jan. 1988.
[21] S. Klein, and G. Nellis, *Heat Transfer*. Cambridge University Press, 2008.
[22] T. Fang and W. Jing, “Flow, heat and species transfer over a stretching plate considering coupled Stefan blowing effects from species transfer,” *Commun. Nonlinear Sci. Numer. Simul.*, vol. 19, no. 9, pp. 3086–3097, Sep. 2014.
[23] M. J. Uddin, M. N. Kabir, and O. A. Bég, “Computational investigation of Stefan blowing and multiple-slip effects on buoyancy-driven bioconvection nanofluid flow with microorganisms,” *Int. J. Heat Mass Transf.*, vol. 95, pp. 116–130, Apr. 2016.
[24] N. A. Latiff, M. J. Uddin, and A. I. M. Ismail, “Stefan blowing effect on bioconvective flow of nanofluid over a solid rotating stretchable disk,” *Propuls. Power Res.*, vol. 5, no. 4, pp. 267–278, Dec. 2016.
[25] P. Rana, N. Shukla, O. A. Beg, A. Kadir, and B. Singh, “Unsteady electromagnetic radiative nanofluid stagnation-point flow from a stretching sheet with chemically reactive nanoparticles, Stefan blowing effect and entropy generation,” *Proc. Inst. Mech. Eng. Part N J. Nanomater. Nanoeng. Nanosyst.*, Jun. 2018.
[26] A. Bejan, “Method of entropy generation minimization, or modeling and optimization based on combined heat transfer and thermodynamics,” *Rev. Générale Therm.*, vol. 35, no. 418, pp. 637–646, Nov. 1996.
[27] M. H. Abolbashari, N. Freidoonimehr, F. Nazari, and M. M. Rashidi, “Entropy analysis for an unsteady MHD flow past a stretching permeable surface in nano-fluid,” *Powder Technol.*, vol. 267, pp. 256–267, Nov. 2014.
[28] A. S. Butt, S. Munawar, A. Ali, and A. Mehmood, “Entropy generation in the Blasius flow under thermal radiation,” *Phys. Scr.*, vol. 85, no. 3, p. 035008(1-6), Mar. 2012.
[29] J. Qing, M. Bhatti, M. Abbas, M. Rashidi, and M. Ali, “Entropy generation on MHD Casson nanofluid flow over a porous stretching/shrinking surface,” *Entropy*, vol. 18, no. 4, pp. 1–14, Apr. 2016.

[30] M. Bhatti, T. Abbas, M. Rashidi, and M. Ali, "Numerical Simulation of Entropy Generation with Thermal Radiation on MHD Carreau Nanofluid towards a Shrinking Sheet," *Entropy*, vol. 18, no. 6, p. 200, May 2016.
[31] S. Aïboud and S. Saouli, "Second law analysis of viscoelastic fluid over a stretching sheet subject to a transverse magnetic field with heat and mass transfer," *Entropy*, vol. 12, no. 8, pp. 1867–1884, Jul. 2010.
[32] M. Bhatti *et al.*, "Entropy Generation on MHD Eyring–Powell Nanofluid through a Permeable Stretching Surface," *Entropy*, vol. 18, no. 6, p. 224, Jun. 2016.
[33] S. J. Liao, *Homotopy analysis method in nonlinear differential equations*. Beijing: Higher Education Press, 2012.
[34] F. Mabood, W. A. Khan, and A. I. M. Ismail, "MHD flow over exponential radiating stretching sheet using homotopy analysis method," *J. King Saud Univ. - Eng. Sci.*, vol. 29, no. 1, pp. 68–74, Jan. 2017.
[35] I. A. Abdallah, "Homotopy analytical solution of MHD fluid flow and heat transfer problem," *Appl Math Inf Sci*, vol. 3, no. 2, pp. 223–233, 2009.
[36] M. J. Uddin, Y. Alginahi, O. A. Bég, and M. N. Kabir, "Numerical solutions for gyrotactic bioconvection in nanofluid-saturated porous media with Stefan blowing and multiple slip effects," *Comput. Math. Appl.*, vol. 72, no. 10, pp. 2562–2581, Nov. 2016.
[37] B. C. Pak and Y. I. Cho, "Hydrodynamic and Heat Transfer Study of Dispersed Fluids with Submicron Metallic Oxide Particles," *Exp. Heat Transf.*, vol. 11, no. 2, pp. 151–170, Apr. 1998.
[38] S. J. Liao, *Beyond Perturbation: Introduction to the Homotopy Analysis Method*. Chapman & Hall/CRC Press, London/Boca Ratton, 2003.

Table 1 Thermo-physical properties of water, Al_2O_3 and TiO_2 particles[19]

	$k\left(Wm^{-1}K^{-1}\right)$	$\rho\left(kgm^{-3}\right)$	$C_p\left(Jkg^{-1}K^{-1}\right)$	$D_B\left(m^2s^{-1}\right)$	$D_T\left(m^2s^{-1}\right)$
Al_2O_3	40	3970	765	4×10^{-11}	6×10^{-11}
TiO_2	8.9538	4250	686.2	4×10^{-11}	6×10^{-11}
Pure water	0.613	997.1	4179	–	–

Table-2 Rate of Convergence of HAM Solution

Order of approximation (terms)	$\{f''(0)\}$	$\{\theta(0)\}$	$\phi(0)$
10	0.9824	0.9188	0.4930
15	0.9841	0.9213	0.4937
18	0.9846	0.9223	0.4940
20	0.9849	0.9228	0.4942
22	0.9851	0.9233	0.4944
25	0.9853	0.9236	0.4945

Table-3 Code validation of HAM results with shooting results

		$\{-f''(0)\}$		$\{-\theta'(0)\}$		$\{\phi(0)\}$	
D	*Sc*	HAM	Shooting	HAM	Shooting	HAM	Shooting
	10	0.1466	0.1455	0.7545	0.7525	0.4945	0.4978
0.01	15	0.1498	0.1453	0.7513	0.7521	0.4950	0.4981
	20	0.1494	0.1452	0.7507	0.7518	0.4954	0.4983
0.003	10	0.1429	0.1498	0.7493	0.7494	0.4983	0.4993
0.005		0.1443	0.1449	0.7519	0.7512	0.4971	0.4989

FIGURES

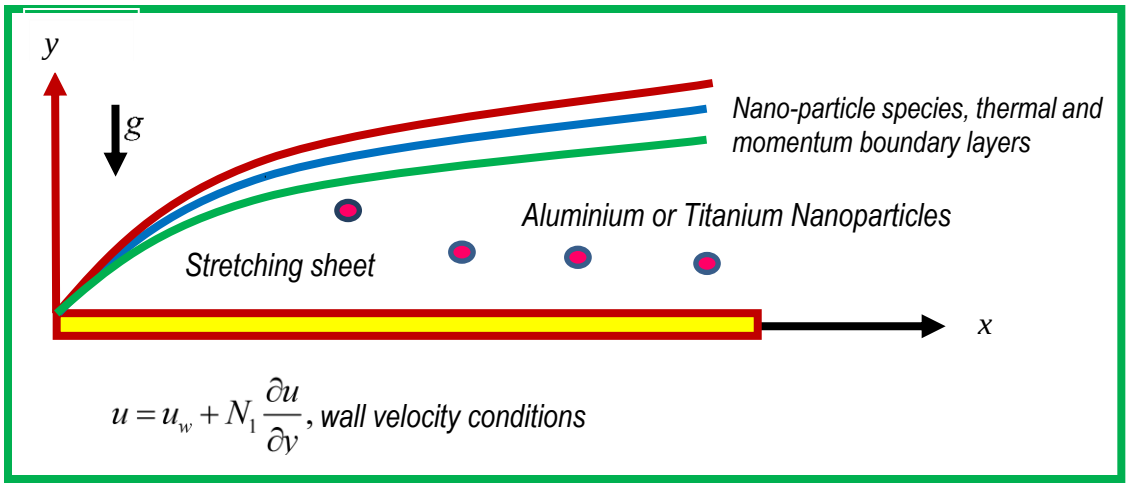

Fig. 1: Coordinate system and flow model.

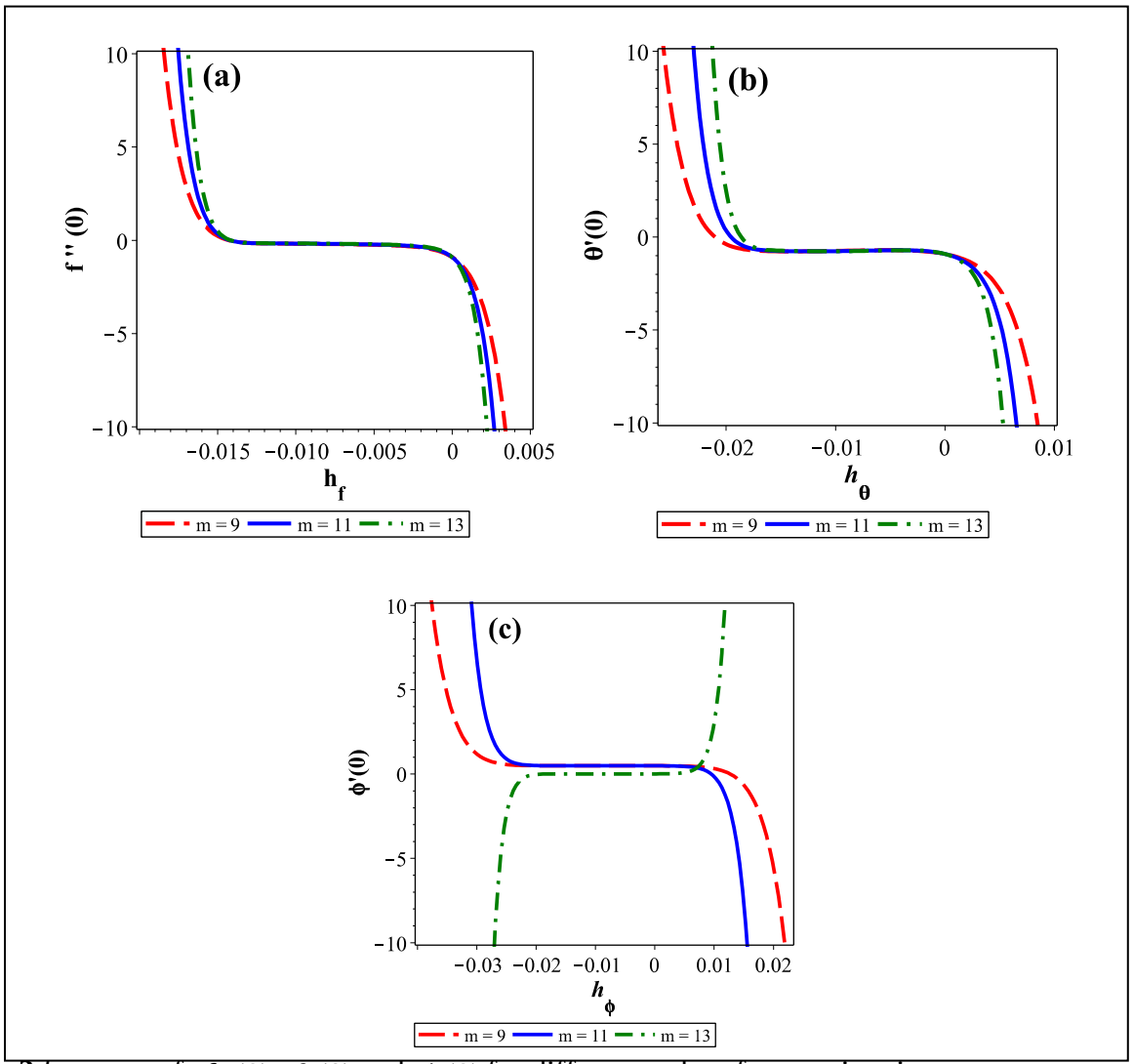

Fig. 2 *h-curves* of $f''(0)$, $\theta'(0)$ and $\phi'(0)$ for different order of approximations.

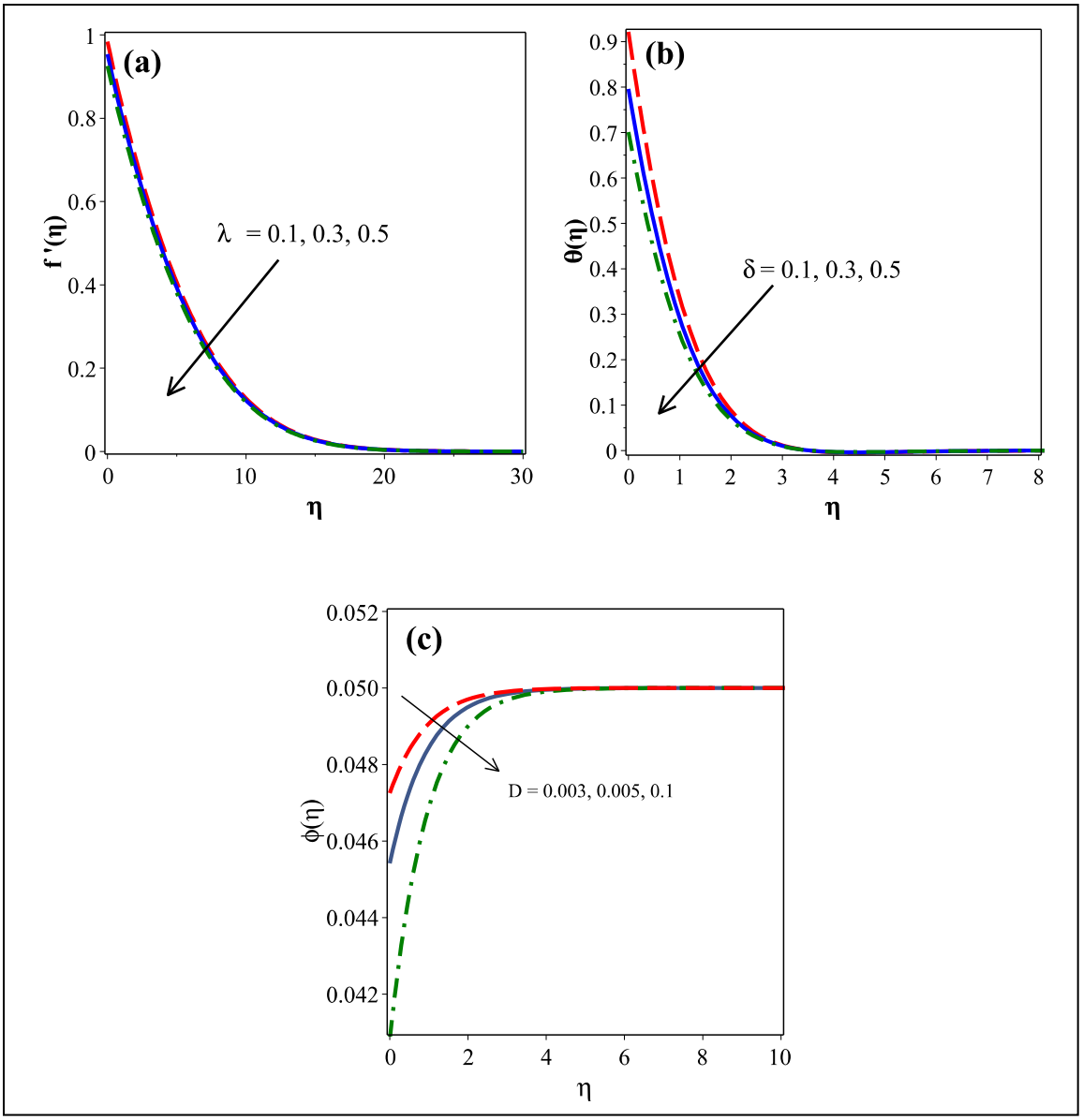

Fig. 3 Effect of λ on velocity, δ on temperature and D on concentration of nanoparticles.

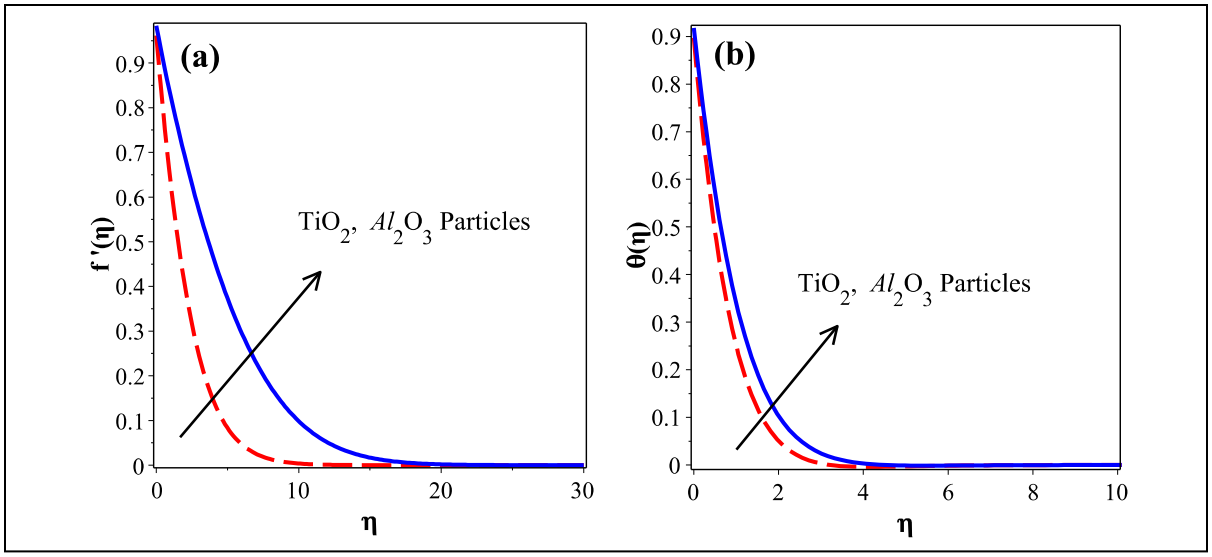

Fig.4 Velocity and temperature profiles for Al_2O_3 and TiO_2 water nanofluid.

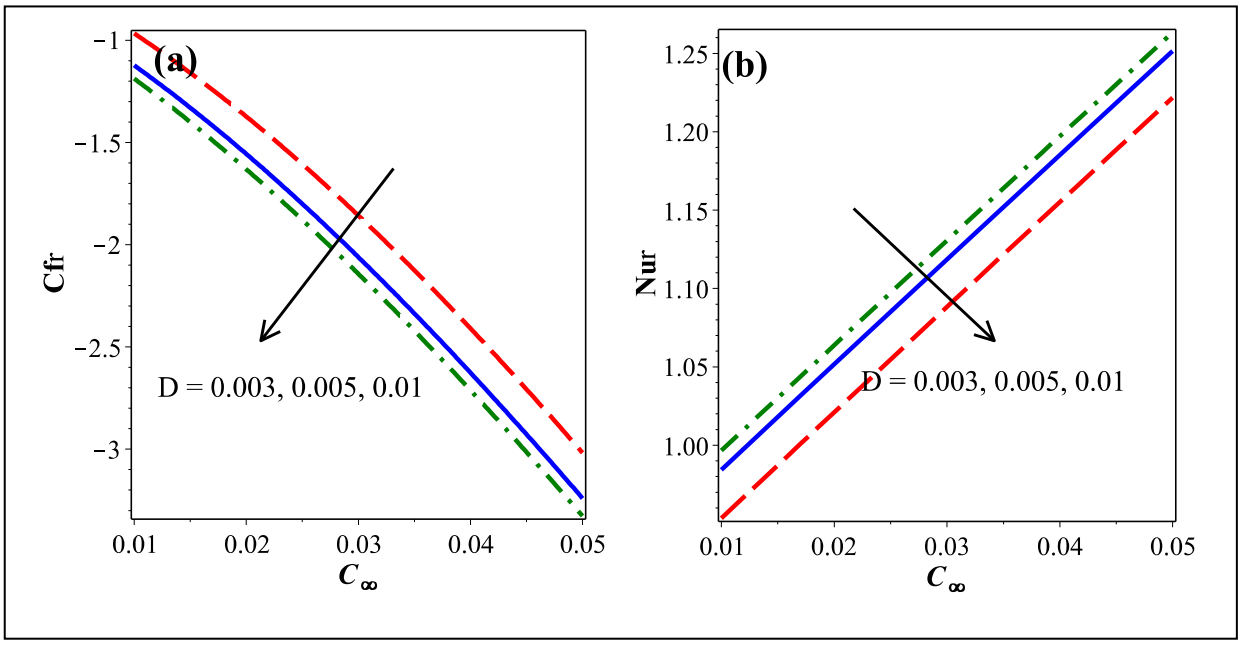

Fig. 5 Combined effect of *D* and C_∞ on skin friction coefficient and Nusselt number.

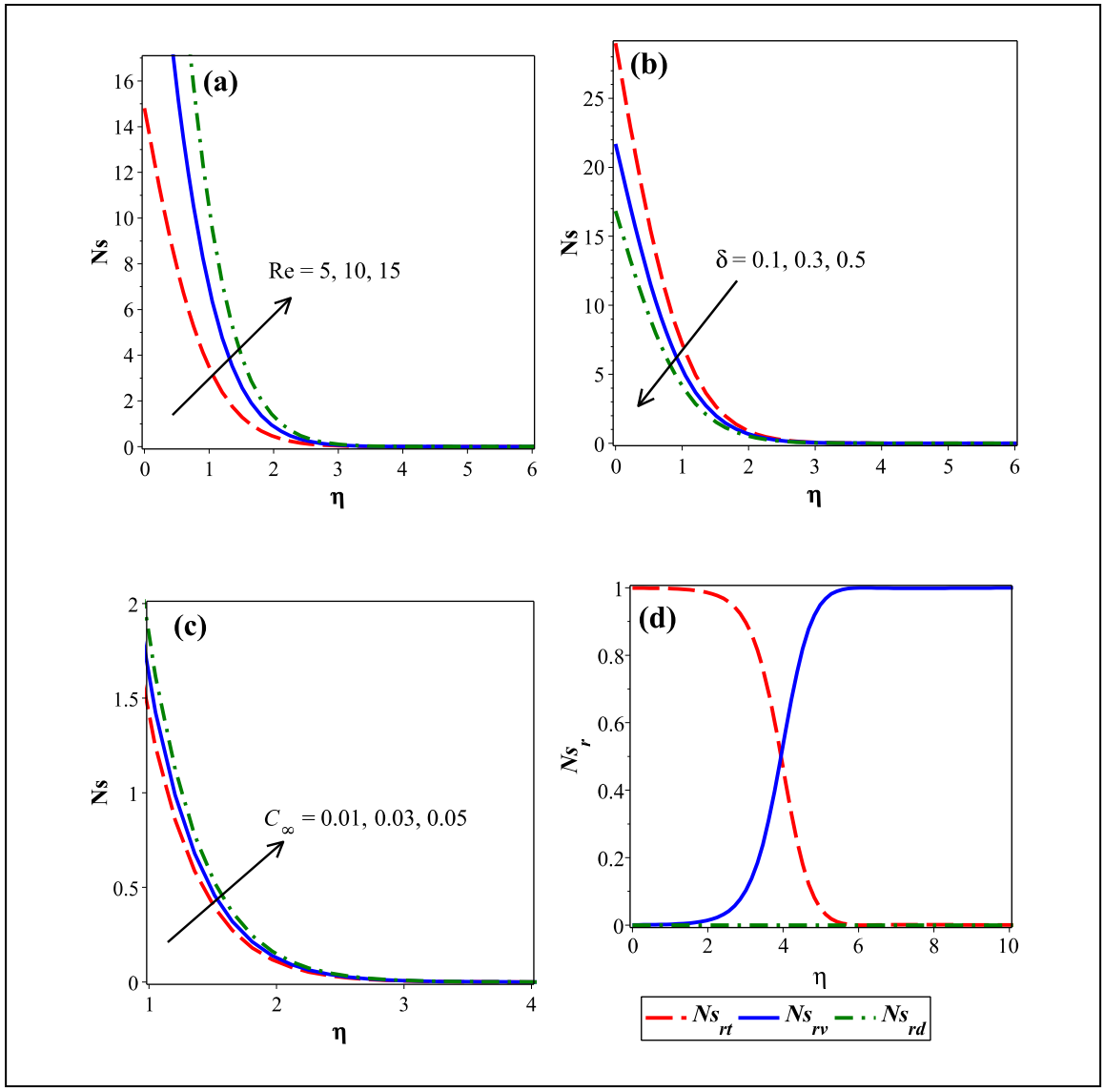

Fig.6 Effect of physical parameters Re, $\mathcal{S}$ and C_∞ on entropy generation number and relative entropy generation number.

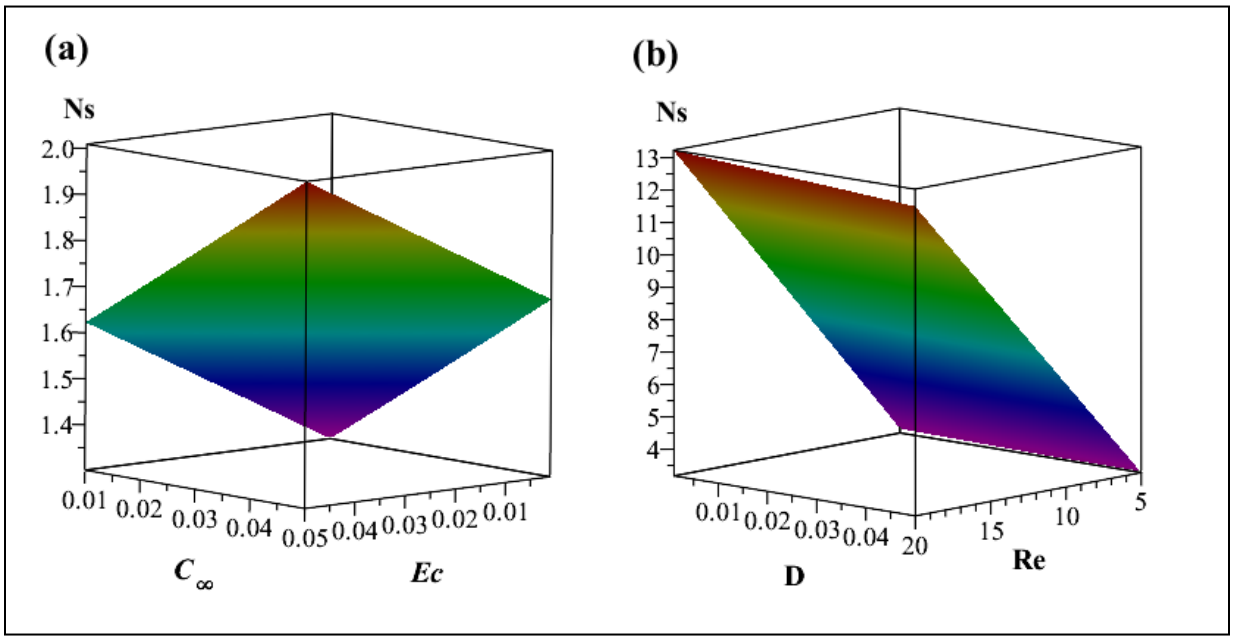

Fig.7 Combined effect of $(Ec,\ C_\infty)$ and $(\mathrm{Re},\ \mathrm{D})$ on entropy generation number.